# A robust and rapid numerical method for dispersive models admitting a lagrangian : application to Serre-Green-Naghdi equations for long free surface gravity waves

N Favrie, S Gavrilyuk

# A robust and rapid numerical method for dispersive models admitting a lagrangian : application to Serre-Green-Naghdi equations for long free surface gravity waves

N. Favrie[*], S. Gavrilyuk[†]

September 1, 2016

**Abstract**

A new numerical method for solving the Serre-Green-Naghdi (SGN) equations describing dispersive waves on shallow water is proposed. From the mathematical point of view, the SGN equations are the Euler-Lagrange equations for a 'master' lagrangian submitted to a differential constraint which is the mass conservation law. One major numerical challenge in solving the SGN equations is the resolution of an elliptic problem at each time instant. It is the most time-consuming part of the numerical method. The idea is to replace the 'master' lagrangian by a one-parameter family of 'extended' lagrangians, for which the corresponding Euler - Lagrange equations are hyperbolic. In such an approach, the 'master' lagrangian is recovered by the 'extended' lagrangian in some limit (for example, when the corresponding parameter is large). The choice of such a family of extended lagrangians is proposed and discussed. The corresponding hyperbolic system is numerically solved by a Godunov type method. Numerical solutions are compared with exact solution of the SGN equations. It appears that the computational time in solving the hyperbolic system is much lower than in the case where the elliptic operator is inverted. The new method is, in particular, applied to study the 'Favre waves' which are non-stationary undular bores produced after reflection of the fluid flow with a free surface at an immobile wall.

**Keywords:** dispersive equations, hyperbolicity, Godunov-type methods

## 1 Introduction

Dispersive systems of equations appearing in physics often admit a variational formulation. Numerous physical examples can be found in the literature : water waves, quantum mechanics, solid mechanics, capillary fluids, bubbly fluids, etc. (cf. [32], [1], [30], [8], [2], [15]). Even if the physics is better captured by the dispersive models, the mathematical and numerical study of such models represents a difficult problem. One example is the Serre-Green-Naghdi equations (SGN equations) describing dispersive water waves [27], [17], [18], [29]. In particular, the inversion of an elliptic operator is needed at each time step when the model is numerically solved [20], [22]. As a consequence, this drastically increases the calculation time. An analogous approach

[*]Aix-Marseille Université, UMR CNRS 7343, IUSTI, 5 rue E. Fermi, 13453 Marseille Cedex 13, France, nicolas.favrie@univ-amu.fr

[†]Corresponding author : Aix-Marseille Université, UMR CNRS 7343, IUSTI, 5 rue E. Fermi, 13453 Marseille Cedex 13, France and Novosibirsk State University, 2 Pirogova street, 630090 Novosibirsk, Russia, sergey.gavrilyuk@univ-amu.fr

was also applied in [25] for a linearised version of the SGN equations (Boussinesq equations). Another important numerical problem is how to impose artificial non-reflecting (transparent) conditions at the boundary of the calculation region for dispersive equations. The transparent boundary conditions are important when one looks for waves passing through a bounded numerical domain. This is always an open problem for general dispersive equations. Some progress was recently done for scalar dispersive equations (Korteweg-de Vries et Benjamin-Bona-Mahony equations) [3], [4]. However, in the theory of hyperbolic equations the last question is solved, at least for homogeneous systems of equations (see [19], for example). Indeed, to avoid the wave reflection, it is necessary just to 'kill' the Riemann invariants corresponding to the characteristics which enter the domain of calculation. A natural idea is thus to replace dispersive equations by approximate hyperbolic equations. The idea is not new and comes from the pioneering work by Cattaneo [5] who replaced, in particular, the heat equation by a hyperbolic system of equations with relaxation. A recent important development of such an approach to dissipative continuum mechanics models can be found in [26] and [7]. However, such an approach can not be satisfactory when the governing equation are the Euler-Lagrange equations for some 'master' lagrangian. Indeed, the energy should be conserved, while it decreases when the relaxation is added. An idea consists to consider an 'extended' lagrangian where some gradients or temporal derivatives of unknowns are replaced by new variables that become true gradients or temporal derivatives only in some limit (to be precised). Such a limit is not a viscous Cattaneo type limit, because the energy of the system is conserved, but a 'non-viscous' limit allowing to 'spread' the energy of the 'master' system into additional degrees of freedom. This approach is reminiscent of the modeling of micromorphic materials ([9], [21], [11], [12]) when it is restricted to reversible processes. The formulation of the extended lagrangian as a function of usual macroscopic and new dual variables is a rather intuitive procedure because the choice of the lagrangian is not unique. Also, some obvious constraints should be satisfied when such a lagrangian is constructed. Indeed,

- At least a one-parameter family of 'extended' lagrangians should be properly choosen, giving in some limit (for example, when the parameter goes to infinity) the 'master' lagrangian.
- The Euler-Lagrange equations for the 'extended' lagrangian should be unconditionally hyperbolic. It means that the corresponding Cauchy problem is well posed. If the equations are only conditionally hyperbolic, additional numerical problems can appear.
- In the linear approximation, the Whitham type condition [32] should be satisfied : the phase velocities of waves corresponding to the 'master ' lagrangian should be interplaced between the phase velocities corresponding to the 'extended' lagrangian for any wave numbers. This condition is well known in hyperbolic equations where it is often called 'subcharacteristic' condition. In particular, it implies the linear stability of equilibrium solutions. Such a condition should also be satisfied for dispersive equations. In particular, it allows us to split the propagation wave modes and understand which one is responsible for the dispersive properties of the limit system.

Some optimisation is thus needed to choose an 'extended' lagrangian satisfying these properties.

In Section 2, the SGN equations are presented. An 'extended' lagrangian and the corresponding Euler-Lagrange equations are formulated in Section 3. A numerical method and numerical results are given in Sections 4 and 5. Technical detail are given in Appendix.

# 2 The SGN equations

Consider the one-dimensional SGN equations describing dispersive non-linear long water waves in a one layer flow over a flat bottom. The dissipative effects are neglected. Under these assumptions

the equations read :

$$\begin{array}{l} \dfrac{\partial h}{\partial t} + \dfrac{\partial hu}{\partial x} = 0, \\ \dfrac{\partial hu}{\partial t} + \dfrac{\partial hu^2 + p}{\partial x} = 0, \text{ with } p = \dfrac{gh^2}{2} + \dfrac{1}{3}h^2\ddot{h}. \end{array} \tag{1}$$

Here $h > 0$ is the total water depth and $u$ is the average horizontal velocity. The 'dots' mean the material derivatives:

$$\dot{h} = \frac{\partial h}{\partial t} + u\frac{\partial h}{\partial x}, \quad \ddot{h} = \left(\frac{\partial}{\partial t} + u\frac{\partial}{\partial x}\right)\dot{h}. \tag{2}$$

The system (1) admits a variational formulation with the lagrangian (see [30],[13], [14], [15]) :

$$\mathcal{L} = \int_{-\infty}^{\infty} \left(\frac{hu^2}{2} - W(h, \dot{h})\right) dx, \tag{3}$$

where the potential is

$$W(h, \dot{h}) = \frac{gh^2}{2} - \frac{h\dot{h}^2}{6}. \tag{4}$$

To simplify the derivation of the governing equations, we will use the mass Lagrangian coordinate $q$ instead of the Eulerian coordinate $x$ :

$$q = \int_0^X h_0(s)ds, \tag{5}$$

where $X$ is the classical Lagrangian coordinate, and $h_0(X)$ is the initial data for the fluid depth. Let $\tau = \dfrac{1}{h}$. The lagrangian reads then:

$$\mathcal{L} = \int_{-\infty}^{\infty} L\, dq, \quad L = \frac{u^2}{2} - \tilde{W}(\tau, \tau_t), \tag{6}$$

with

$$u = x_t, \quad \tau = x_q, \quad \tilde{W}(\tau, \tau_t) = \frac{g}{2\tau} - \frac{1}{6}\left(\frac{\partial 1/\tau}{\partial t}\right)^2. \tag{7}$$

The governing equations in the mass Lagrangian coordinates can be written as :

$$\tau_t - u_q = 0, \quad u_t + p_q = 0, \tag{8}$$

with

$$p = -\frac{\delta \tilde{W}}{\delta \tau} = -\left(\frac{\partial \tilde{W}}{\partial \tau} - \frac{\partial}{\partial t}\left(\frac{\partial \tilde{W}}{\partial \tau_t}\right)\right) = \frac{g}{2\tau^2} + \frac{2}{3}\frac{\tau_t^2}{\tau^5} - \frac{1}{3}\frac{\tau_{tt}}{\tau^4}. \tag{9}$$

They admit the energy conservation law :

$$\left(\frac{u^2}{2} + e\right)_t + (pu)_q = 0, \tag{10}$$

with

$$e = \frac{g}{2\tau} + \frac{1}{6}\frac{\tau_t^2}{\tau^4}. \tag{11}$$

# 3 The method of an 'extended' lagrangian for the SGN equations

Let $\tau = x_q$, and $u = x_t$. We introduce now a non-equilibrium variable $\eta$ having the propriety that in equilibrium, one has $\eta = \frac{1}{\tau}$. We take the extended lagrangian under the following form :

$$\hat{\mathcal{L}} = \int_{-\infty}^{\infty} \hat{L}\, dq, \quad \hat{L} = \frac{x_t^2}{2} + \frac{\eta_t^2}{6} - \frac{g}{2\tau} - \alpha(\tau,\eta)\frac{(\eta - \frac{1}{\tau})^2}{6}. \tag{12}$$

To guarantee the convergence (weak) of the solutions of the Euler-Lagrange equations for the lagrangian (12), to the solutions of the SGN equations (8)-(9), the function $\alpha(\tau,\eta)$ should be quite large. Below, we will precise this function. Let us consider the following three one-parameter lagrangians corresponding to different choice of $\alpha(\tau,\eta)$:

$$\hat{\mathcal{L}} = \int_{-\infty}^{\infty} \hat{L}\, dq, \quad \hat{L} = \frac{x_t^2}{2} + \frac{\eta_t^2}{6} - \frac{g}{2\tau} - \lambda\frac{(\eta - \frac{1}{\tau})^2}{6}, \quad \alpha = \lambda = const > 0. \tag{13}$$

$$\hat{\mathcal{L}} = \int_{-\infty}^{\infty} \hat{L}\, dq, \quad \hat{L} = \frac{x_t^2}{2} + \frac{\eta_t^2}{6} - \frac{g}{2\tau} - \lambda\frac{(\eta\tau - 1)^2}{6}, \quad \alpha = \lambda\tau^2, \quad \lambda = const > 0. \tag{14}$$

$$\hat{\mathcal{L}} = \int_{-\infty}^{\infty} \hat{L}\, dq, \quad \hat{L} = \frac{x_t^2}{2} + \frac{\eta_t^2}{6} - \frac{g}{2\tau} - \lambda\frac{(\eta\tau - 1)^4}{6}, \quad \alpha = \lambda\tau^2(\eta\tau - 1)^2, \quad \lambda = const > 0. \tag{15}$$

In all the cases (13) - (15) the parameter $\lambda$ is large.

## 3.1 First lagrangian $\alpha(\eta,\tau) = \lambda$

We consider first the extended lagrangian (13). The corresponding Euler-Lagrange equations read :

$$\begin{cases} -\dfrac{\partial}{\partial t}\left(\dfrac{\partial \hat{L}}{\partial x_t}\right) - \dfrac{\partial}{\partial q}\left(\dfrac{\partial \hat{L}}{\partial x_q}\right) = 0, \\ \dfrac{\partial \hat{L}}{\partial \eta} - \dfrac{\partial}{\partial t}\left(\dfrac{\partial \hat{L}}{\partial \eta_t}\right) = 0. \end{cases} \tag{16}$$

Complemented with the mass conservation law which is just the compatibility condition $\tau_t - u_q = 0$ with $\tau = x_q$ and $u = x_t$, they can be rewritten as :

$$\begin{cases} \tau_t - u_q = 0, \\ u_t - \left(\dfrac{g}{\tau^3} + \dfrac{\lambda}{\tau^3}\left(\dfrac{1}{\tau} - \dfrac{2}{3}\eta\right)\right)\tau_q - \dfrac{\lambda}{3}\dfrac{\eta_q}{\tau^2} = 0, \\ \eta_{tt} = \lambda\left(\dfrac{1}{\tau} - \eta\right). \end{cases} \tag{17}$$

This system can be rewritten in conservative form :

$$\begin{cases} \tau_t - u_q = 0, \\ u_t + \left(\dfrac{g}{2\tau^2} + \dfrac{\lambda}{3\tau^2}\left(\dfrac{1}{\tau} - \eta\right)\right)_q = 0, \\ \eta_t = w, \\ w_t = \lambda\left(\dfrac{1}{\tau} - \eta\right). \end{cases} \tag{18}$$

The characteristic slopes are :

$$\xi_{1,2} = 0, \quad \xi_{3,4} = \pm\sqrt{\frac{g}{\tau^3} + \frac{\lambda}{\tau^3}\left(\frac{1}{\tau} - \frac{2}{3}\eta\right)}. \tag{19}$$

This model is hyperbolic if $\eta < \frac{3}{2}\left(\frac{g}{\lambda} + \frac{1}{\tau}\right)$. This system is similar to the one proposed by Liapidevskii and Gavrilova (2008) [23] where a different approach based on the averaging of instantaneous variables was used. Due to the Noether theorem, system (18) admits the energy conservation law :

$$\left(\frac{u^2}{2} + \frac{w^2}{6} + \frac{g}{2\tau} + \lambda\frac{(\eta\tau - 1)^2}{6\tau^2}\right)_t + (pu)_q = 0, \quad p = \frac{g}{2\tau^2} + \frac{\lambda}{3\tau^2}\left(\frac{1}{\tau} - \eta\right).$$

The system (18) is only conditionally hyperbolic, so it does not fully satisfies all the constraints mentioned in the Introduction.

### 3.2 Second lagrangian $\alpha(\tau, \eta) = \lambda\tau^2$

Consider now the extended lagrangian (14). The Euler-Lagrange equations imply :

$$\begin{cases} u_t - \left(\frac{g}{\tau^3} + \frac{\lambda}{3}\eta^2\right)\tau_q - \frac{\lambda}{3}(2\tau\eta - 1)\eta_q = 0, \\ \eta_{tt} = -\lambda\left(\eta\tau - 1\right)\tau. \end{cases} \tag{20}$$

This system can be rewritten in conservative form :

$$\begin{cases} \tau_t - u_q = 0, \\ u_t + \left(\frac{g}{2\tau^2} - \frac{\lambda}{3}(\tau\eta - 1)\eta\right)_q = 0, \\ \eta_t = w, \\ w_t = -\lambda\left(\eta\tau - 1\right)\tau. \end{cases} \tag{21}$$

This system is unconditionally hyperbolic, the characteristic slopes are :

$$\xi_{1,2} = 0, \quad \xi_{3,4} = \pm\sqrt{\frac{g}{\tau^3} + \frac{\lambda}{3}\eta^2} \tag{22}$$

System (21) admits the energy conservation law :

$$\left(\frac{u^2}{2} + \frac{w^2}{6} + \frac{g}{2\tau} + \lambda\frac{(\eta\tau - 1)^2}{6}\right)_t + (pu)_q = 0, \quad p = \frac{g}{2\tau^2} - \frac{\lambda}{3}\left(\tau\eta - 1\right)\eta.$$

For the original Green-Naghdi model the phase velocity $c_p = \omega/k$ of the linear waves linearized at $u = 0, \tau = \tau_0$ is :

$$c_p^2 = \frac{g}{\tau_0^3 + \frac{k^2}{3\tau_0}} \tag{23}$$

For the new model, the phase velocity reads (see Appendix for details):

$$\left(c_p^{\pm}\right)^2 = \frac{\frac{g}{\tau_0^3} + \frac{\lambda}{3\tau_0^2} + \frac{\lambda\tau_0^2}{k^2} \pm \sqrt{\left(\frac{g}{\tau_0^3} + \frac{\lambda}{3\tau_0^2} + \frac{\lambda\tau_0^2}{k^2}\right)^2 - 4\frac{g\lambda}{\tau_0 k^2}}}{2}. \tag{24}$$

The phase velocity corresponding to the sign 'minus' ('plus') is called *slow* (*rapid*) phase velocity. These phase velocities are interplaced between the phase velocities corresponding to the SGN lagrangian (see Figures 1 and 2), so the Whitham type condition is also satisfied. On can see in Figure 1 that the slow waves correspond to the SGN dispersion relation defined by (23) if $\lambda$ is suficiently large.

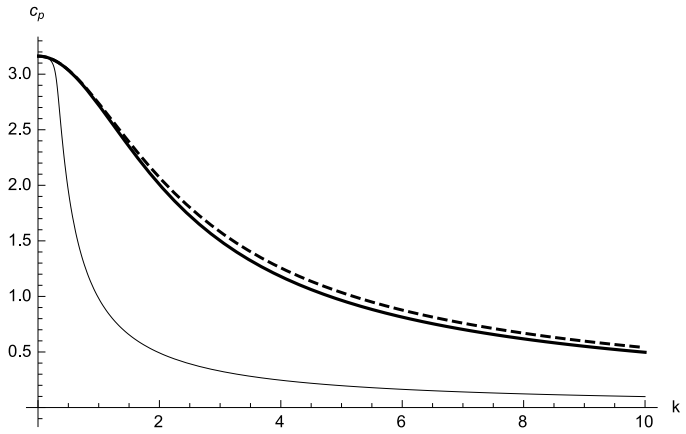


Figure 1: We represent the evolution of the slow phase velocity $c_p^-$ defined by (24) as a function of the wave number $k$ for the SGN (dashed line) and for the new model with $\lambda = 1\ m^2\ s^{-2}$ (thin line) and $\lambda = 160\ m^2\ s^{-2}$ (thick line). The value of $\tau_0$ is $1m^{-1}$. When the parameter $\lambda$ is sufficiently large, the phase velocity is close to that of the original model defined by (23).

### 3.3 Third lagrangian $\alpha(\tau,\eta) = \lambda\tau^2\left(\eta\tau-1\right)^2$

We consider now the extended lagrangian (15). The Euler-Lagrange equations imply:

$$\begin{cases} u_t - \left(\dfrac{g}{\tau^3} + 2\lambda(\eta\tau-1)^2\eta^2\right)\tau_q - \dfrac{2\lambda}{3}(\tau\eta-1)^2(4\tau\eta-1)\eta_q = 0, \\ \eta_{tt} = -2\lambda\left(\eta\tau-1\right)^3\tau. \end{cases} \tag{25}$$

This system can again be rewritten in conservative form :

$$\begin{cases} \tau_t - u_q = 0, \\ u_t + \left(\dfrac{g}{2\tau^2} - \dfrac{2\lambda}{3}(\tau\eta-1)^3\eta\right)_q = 0, \\ \eta_t = w, \\ w_t = -2\lambda\left(\eta\tau-1\right)^3\tau. \end{cases} \tag{26}$$

This system is unconditionally hyperbolic, with the following characteristic slopes :

$$\xi_{1,2} = 0, \quad \xi_{3,4} = \pm\sqrt{\frac{g}{\tau^3} + 2\lambda(\eta\tau-1)^2\eta^2}. \tag{27}$$

System (26) admits the energy conservation law :

$$\left(\frac{u^2}{2} + \frac{w^2}{6} + \frac{g}{2\tau} + \lambda\frac{(\eta\tau-1)^4}{6}\right)_t + \left(pu\right)_q = 0, \quad p = \frac{g}{2\tau^2} - \frac{2\lambda}{3}\left(\tau\eta-1\right)^3\eta.$$

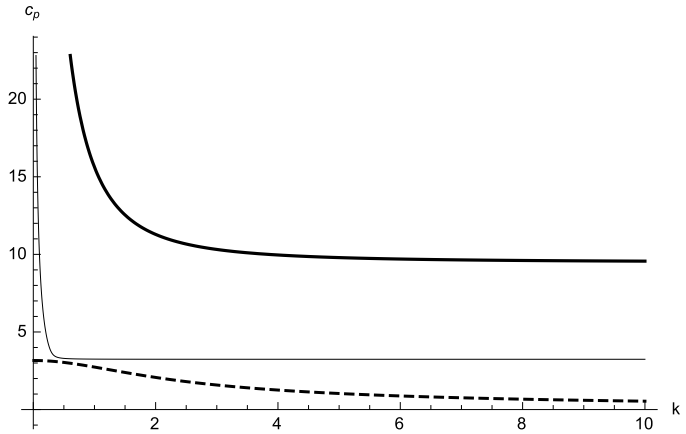


Figure 2: We represent the evolution of the rapid phase velocity $c_p^+$ as a function of the wave number $k$ for the SGN equations (dashed line) and for the new model with $\lambda = 1\ m^2\ s^{-2}$ (thin line) and $\lambda = 160\ m^2\ s^{-2}$ (thick line). The value of $\tau_0$ is $1m^{-1}$. This velocity is always higher then that of the original model. It describes the evolution of 'parasitic' high-frequency waves related to the modification of the lagrangian.

The phase velocity of linear waves does not depend on the wave number :

$$c_p^2 = \frac{g}{\tau^3}. \tag{28}$$

Since the dispersion effects are not captured in the linear approximation, the model is not able to deal with an accurate description of the SGN equations. In the following, we will concentrate on the numerics of the Euler-Lagrange equations (21) obtained from the lagrangian (14).

# 4 Numerical resolution

The lagrangian form of system (21) is :

$$\frac{\partial \tilde{\mathbf{U}}}{\partial t} + \frac{\partial \tilde{\mathbf{F}}}{\partial q} = \tilde{\mathbf{S}}, \tag{29}$$

with $\tilde{\mathbf{U}} = (\tau, u, \eta, w)^T$, $\tilde{\mathbf{F}} = \left(-u, \frac{g}{2\tau^2} - \frac{\lambda}{3}(\tau\eta - 1)\eta, 0, 0\right)^T$ and $\tilde{\mathbf{S}} = (0, 0, w, -\lambda\tau(\eta\tau - 1))^T$. The Eulerian form of system (21) is :

$$\frac{\partial \mathbf{U}}{\partial t} + \frac{\partial \mathbf{F}}{\partial x} = \mathbf{S}, \tag{30}$$

with $\mathbf{U} = (h, hu, h\eta, hw)^T$, $\mathbf{F} = \left(hu, hu^2 + \frac{gh^2}{2} - \frac{\lambda}{3}(\frac{\eta}{h} - 1)\eta, h\eta u, hwu\right)^T$ and $\mathbf{S} = \left(0, 0, hw, -\lambda(\frac{\eta}{h} - 1)\right)^T$. In the following, we will use the Eulerian form (30) to have a possibility to compare the numerical results with other numerical approaches. Since, the system is hyperbolic and conservative, a classical Godunov- type method can be used followed by the Strang splitting strategy. Equation (30) is split into a hyperbolic part :

$$\frac{\partial \mathbf{U}}{\partial t} + \frac{\partial \mathbf{F}}{\partial x} = 0, \tag{31}$$

and an ODE part (the treatment of the right-hand side $\mathbf{S}$):

$$\frac{\partial \mathbf{U}}{\partial t} = \mathbf{S}. \tag{32}$$

The operators associated with the discretization of (31) and (32) are denoted $\mathbf{H}_h$ and $\mathbf{H}_r$, respectively. The second-order Strang splitting procedure is used, solving successively (31) and (32) with adequate time increments:

$$\begin{cases} \mathbf{U}_i^{(1)} = \mathbf{H}_r\left(\dfrac{\Delta t}{2}\right)\mathbf{U}_i^n, \\ \mathbf{U}_i^{(2)} = \mathbf{H}_r\left(\Delta t\right)\mathbf{U}_i^{(1)}, \\ \mathbf{U}_i^{n+1} = \mathbf{H}_r\left(\dfrac{\Delta t}{2}\right)\mathbf{U}_i^{(2)}. \end{cases} \tag{33}$$

Since $\mathbf{H}_h$ and $\mathbf{H}_r$ are of second order accuracy operators, the procedure (33) gives us a second-order accuracy approximation of (30) [24].

## 4.1 Hyperbolic step

The equation (31) is solved by a conservative scheme for hyperbolic systems [24]

$$\mathbf{U}_i^{n+1} = \mathbf{U}_i^n - \frac{\Delta t}{\Delta x}\left(\mathbf{F}^*_{i+1/2} - \mathbf{F}^*_{i-1/2}\right) \tag{34}$$

The numerical flux function $\mathbf{F}_{i+1/2}$ is computed by using the Rusanov method [28]:

$$\mathbf{F}_{i+1/2} = \frac{1}{2}\left(\mathbf{F}(\mathbf{U}_{i+1}^n) - \mathbf{F}(\mathbf{U}_i^n) - \kappa^n_{i+1/2}(\mathbf{U}_{i+1}^n + \mathbf{U}_i^n)\right) \tag{35}$$

The parameter $\kappa^n_{i+1/2}$ is obtained by using the Davis approximation [6] :

$$\kappa^n_{i+1/2} = \max(|c_{i+1}|, |c_i|), \tag{36}$$

where $c_i$ are eigenvalues of the system (30). The usual Courant-Friedrichs-Lewy (CFL) condition is satisfied

$$\Delta t = CFL\frac{\Delta x}{|c_{max}|}, \text{ with } CFL < 1, \tag{37}$$

where $c_{max}$ is a maximal value of the characteristic velocities over the mesh.

## 4.2 ODE step

The source terms treatment is reduced to a second order ordinary differential equation with constant coefficients which can be solved exactly. Indeed, for system (21), the relaxation system (32) is :

$$\begin{aligned} \frac{\partial u}{\partial t} &= 0, \\ \frac{\partial \tau}{\partial t} &= 0, \\ \frac{\partial \eta}{\partial t} &= w, \\ \frac{\partial w}{\partial t} &= \lambda\left(1 - \eta\tau\right)\tau. \end{aligned} \tag{38}$$

It comes :

$$
\begin{aligned}
u(t+dt) &= u(t), \quad \tau(t+dt) = \tau(t), \\
\eta(t+dt) &= \left(\eta(t) - \frac{1}{\tau(t)}\right) cos(\tau(t)\sqrt{\lambda}dt) + \frac{w(t)}{\tau(t)\sqrt{\lambda}} sin(\tau(t)\sqrt{\lambda}dt) + \frac{1}{\tau(t)}, \\
w(t+dt) &= \left(-\tau(t)\sqrt{\lambda}\left(\eta(t) - \frac{1}{\tau(t)}\right) sin(\tau(t)\sqrt{\lambda}dt) + w(t)cos(\tau(t)\sqrt{\lambda}dt)\right).
\end{aligned}
\tag{39}
$$

# 5 Numerical results

## 5.1 Solitary wave solutions

Solitary wave solutions to the SGN system of the form $(h(\xi), u(\xi))$ where $\xi = x - Dt$ and $D$ is a constant wave velocity, are :

$$
\begin{aligned}
h(\xi) &= h_1 + (h_2 - h_1) sech^2\left(\frac{\xi}{2}\sqrt{\frac{3(h_2-h_1)}{h_2 h_1^2}}\right), \\
u(\xi) &= D\left(1 - \frac{h_1}{h(\xi)}\right),
\end{aligned}
\tag{40}
$$

with $D^2 = gh_2$. In the following example, we take $h_1 = 10\ m$, $h_2 = 12.1\ m$ and $g = 10\ m/s^2$. We initialise the density and the velocity with the exact solution and we impose $\eta = h$ and $w = 0$. The maximum of the solitary wave, moving to the right, was initially situated at $x = 200\ m$. One can notice that the initial data is not an exact solution to the extended system. Indeed, the pressure in the SGN system given by $p = \frac{1}{2}gh^2 + \frac{1}{3}h^2\ddot{h}$ is not initially hydrostatic, while it is the case in the extended system. Then the solution of the extended system evolves. In Figure 3, we show the solution for $\lambda = 300\ m^2/s^2$ and $\lambda = 3000\ m^2/s^2$, for the same mesh size $\Delta x = 0.125\ m$. For $\lambda = 3000\ m^2/s^2$ the difference between the exact solution of the SGN equations and the numerical solution corresponding to the 'extended' Lagrangian is almost invisible with the naked eye.

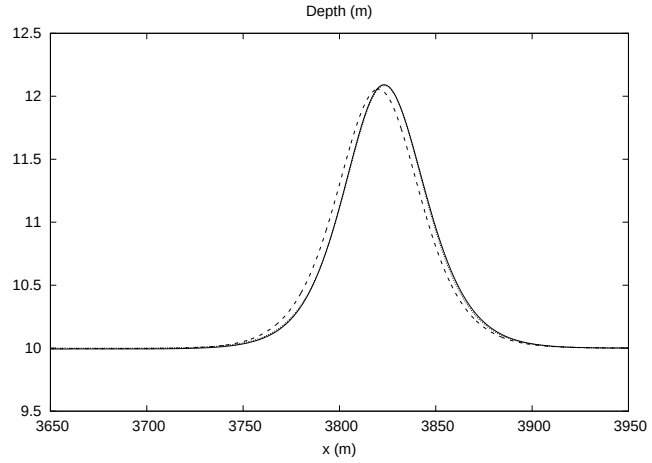


Figure 3: Comparison of the solitary wave solution corresponding to $\lambda = 300$ (dashed line) and $\lambda = 3000$ (dots) with the exact solitary wave solution of the SGN equation (thin curve). The difference between exact solution and that corresponding to $\lambda = 3000$ is almost invisible. The mesh size $\Delta x = 0.125\ m$.

### 5.2 Favre waves

We consider the experiment where a fluid layer with a free surface is impacting a wall ('water hammer problem with a free surface') [10], [31]. Due to dispersion, the reflected wave is rather a wave train of waves of different lengths and amplitudes (called also 'Favre waves', see Figure 4). The SGN equations can be used to model this problem until some critical impact velocity determined in terms of the relative (with respect to the velocity of the reflected wave) Froude number $F$. Above this critical value, the model is no more valid because of the wave breaking (see details in [16]). To avoid the difficulties related to the wall boundary conditions, we consider a symmetric impact test problem. The impact velocity $u_0$ is related to the Froude number $F$ by the formula :

$$u_0 = \sqrt{gh_0}\left(F - \frac{1+\sqrt{1+8F^2}}{4F}\right)$$

In Figure 5, we compare the numerical results at time $t = 54\ s$ with the results obtained by the method [20]. The continuous blue line corresponds to the numerical solution of the SGN equations obtained by the method [20] on a 32000 cells mesh. Our results (second order extension with Van Leer Limiter) were obtained on different meshes (2000, 4000 and 8000 cells) (see Figure 5). The convergence is clearly visible. A good estimation of the first wave amplitude can be obtained with a coarser mesh. In Table 6, we show the computational time for the different mesh sizes. In

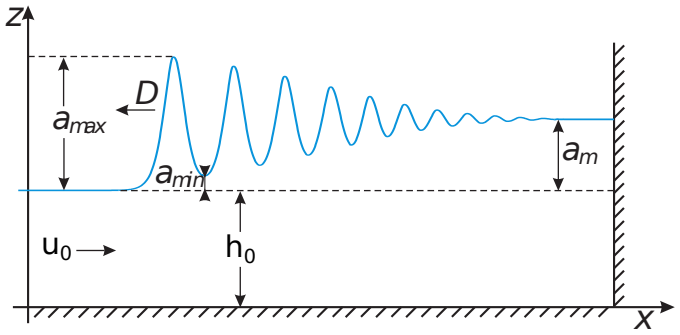


Figure 4: A sketch of Favre waves.

Figure 7, we represent the evolution of the computational time with the mesh size (normalized with the computational time of the coarser grid). One can see that the computational time increases much slower with the mesh refinement for the new hyperbolic approach. Moreover, the new approach is much easier to parallelise by using the domain decomposition methods since equations are hyperbolic. In Figure 8, the numerical results are compared with the experiments of [31]. The results are in perfect agreement until the wave breaking occurs corresponding to the Froude number about 1.25.

## 6 Conclusion

A new numerical approach based on an 'extended' lagrangian is proposed to solve dispersive equations coming from the Euler-Lagrange equations. In particular, this approach transforms the dispersive Serre-Green-Naghdi equations into hyperbolic ones. The computational time is much lower with a new approach, and it's now possible to think about multi-dimensional resolution with a reasonable computational time. Higher order extension based on WENO, ADER or

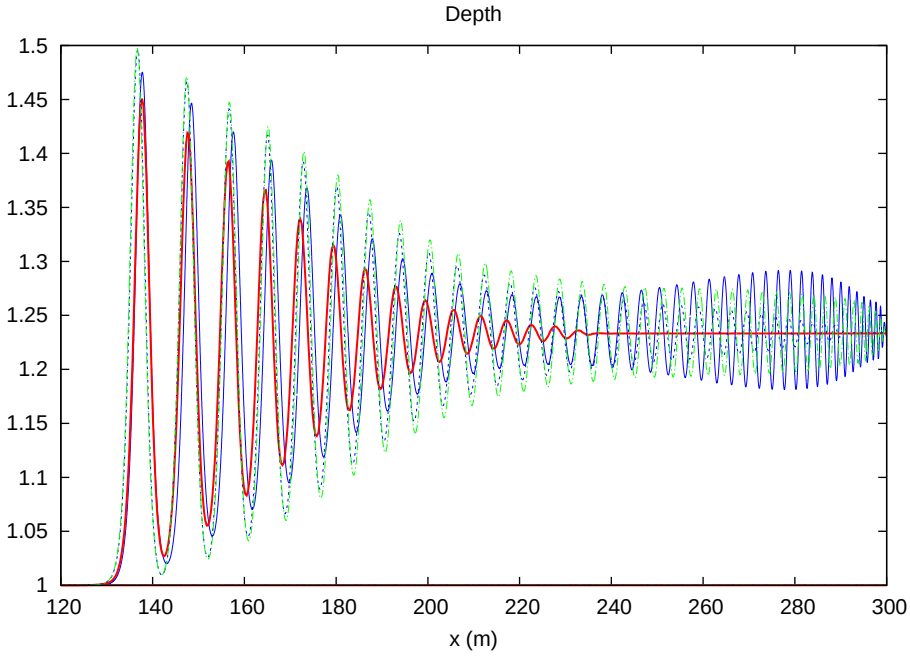


Figure 5: Comparison at time $t = 54s$ for the Froude number $Fr = 1.16$ in the Favre experiment. It corresponds to $h_0 = 1\ m$ and the impact velocity $u_0 = 0.2\sqrt{gh_0}\ m/s$, $g = 10\ m/s$. The result obtained by the method developed in [20] on a 32000 cells mesh is shown with a thin continuous blue line. The results obtained with the second order extension of the new model are shown for different mesh sizes : 2000 (red thick continuous line), 4000 (blue dashed line), 8000 (green dashed-dot line). The agreement is good and the convergence is guaranteed.

| Mesh size | Hyperbolic model | Approach [20] |
|---|---|---|
| 2000 | 1.12 | 12.44 |
| 4000 | 4.65 | 191.84 |
| 8000 | 19.32 | 1844 |
| 16000 | 75.52 | 21200 |

Figure 6: Computational time (in seconds) for the hyperbolic model and for the approach [20].

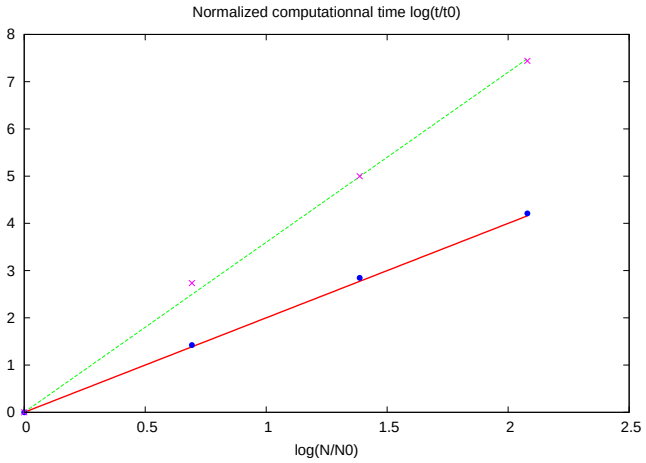


Figure 7: Computational time normalized by $N_0 = 2000$. The crosses correspond to [20], the dots correspond to the hyperbolic method. A thin line has the slope 3.8 while a thick line has a slope 2. The computational time increases much faster for the approach [20].

other methods can be easily developed for this approach. The same approach can also be applied to modelling fluids containing gas bubbles, because the governing equations have the same mathematical structure [13], [14].

**Acknowledgment** This work has been partially supported by the ANR project BoND (Bond-ANR-13-BS01-0009-02) and by the Russian Science Foundation (grant No. 15-11-20013). The authors thank V. Yu. Liapidevskii, A. Madeo and P. Seppecher for helpful discussion.

# A Dispersion relation

We consider the Euler-Lagrange equations for (14) :

$$\begin{cases} \tau_t - u_q = 0, \\ u_t - \left(\dfrac{g}{\tau^3} + \dfrac{\lambda}{3}\eta^2\right)\tau_q - \dfrac{\lambda}{3}(2\tau\eta - 1)\eta_q = 0, \\ \eta_{tt} = -\lambda\left(\eta\tau - 1\right)\tau. \end{cases} \tag{41}$$

Consider the perturbation of a constant state $u = 0$, $\tau = \tau_0$, $\eta = \eta_0$, $\tau_0\eta_0 = 1$ : $u = \varepsilon\tilde{u}$, $\tau = \tau_0 + \varepsilon\tilde{\tau}$, $\eta = \eta_0 + \varepsilon\tilde{\eta}$. At first order the system reads :

$$\begin{cases} \tilde{\tau}_t - \tilde{u}_q = 0, \\ \tilde{u}_t - \left(\dfrac{g}{\tau_0^3} + \dfrac{\lambda}{3}\eta_0^2\right)\tilde{\tau}_q - \dfrac{\lambda}{3}(2\tau_0\eta_0 - 1)\tilde{\eta}_q = 0, \\ \tilde{\eta}_{tt} = -\lambda\left(\tilde{\eta}\tau_0^2 + \tilde{\tau}\right). \end{cases} \tag{42}$$

We consider monochromatic perturbations : $\tilde{u} = u_1 e^{i(kx-\omega t)}$, $\tilde{\tau} = \tau_1 e^{i(kx-\omega t)}$ and $\tilde{\eta} = \eta_1 e^{i(kx-\omega t)}$. We get :

$$\begin{cases} \omega\tau_1 + ku_1 = 0, \\ \omega u_1 + \left(\dfrac{g}{\tau_0^3} + \dfrac{\lambda}{3\tau_0^2}\right)k\tau_1 + \dfrac{\lambda}{3}k\eta_1 = 0, \\ \omega^2\eta_1 - \lambda\left(\eta_1\tau_0^2 + \tau_1\right) = 0. \end{cases} \tag{43}$$

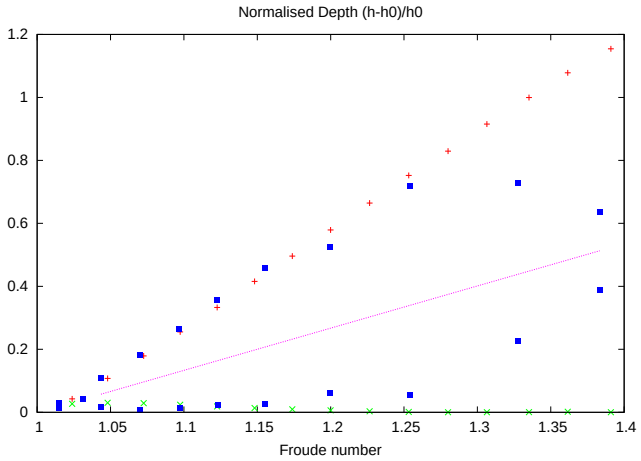


Figure 8: Comparison between the experimental results of [31] (squares) and the numerical results. The upper squares indicate the amplitude of the first wave, while the lower squares show the amplitude of the trough after the first wave. The agreement is perfect until the Froude number about 1.25. After this critical value, the model is no more valid, the wave breaking occurs which is not described by the SGN model (see [16] for better modeling of breaking waves). The middle straight line corresponds to the solution of the Saint-Venant equations.

It can be also written as :

$$\mathbf{A}\mathbf{x} = 0, \quad \mathbf{x}^T = (\tau_1, u_1, \eta_1), \tag{44}$$

with

$$\mathbf{A} = \begin{pmatrix} \omega & k & 0 \\ k\left(\frac{g}{\tau_0^2} + \frac{\lambda}{3\tau_0^2}\right) & \omega & \frac{\lambda k}{3} \\ -\lambda & 0 & \omega^2 - \lambda\tau_0^2 \end{pmatrix}. \tag{45}$$

The corresponding homogeneous linear system has non-trivial solution if and only if the determinant of $\mathbf{A}$ is zero :

$$c_p^4 - c_p^2\left(\frac{g}{\tau_0^3} + \frac{\lambda}{3\tau_0^2} + \frac{\lambda\tau_0^2}{k^2}\right) + \frac{g\lambda}{\tau_0 k^2} = 0. \tag{46}$$

The equation has two real positive roots $c_p^2$ :

$$c_p^2 = \frac{\frac{g}{\tau_0^3} + \frac{\lambda}{3\tau_0^2} + \frac{\lambda\tau_0^2}{k^2} \pm \sqrt{\left(\frac{g}{\tau_0^3} + \frac{\lambda}{3\tau_0^2} + \frac{\lambda\tau_0^2}{k^2}\right)^2 - 4\frac{g\lambda}{\tau_0 k^2}}}{2}. \tag{47}$$

# References


[1] Berdichevskii, V. L. Variational Principles of Continuum Mechanics, Springer Verlag, 2009.

[2] Benzoni-Gavage, S., Noble, P. & Rodrigues, L. M. (2014) Slow modulations of periodic waves in Hamiltonian PDEs, with applications to capillary fluids, J. Nonlinear Science, **24**, N 4, 711-768.

[3] Besse, C., Ehrhardt, M. & Lacroix-Violet (2016) Discrete Artificial Boundary Conditions for the Korteweg-de Vries Equation, Numer. Meth. for PDEs, **33**, 5, p. 1455 - 1484.

[4] Besse, C., Mésognon-Gireauy, B. & Noble, P. (2016) Artificial boundary conditions for the linearized Benjamin-Bona-Mahony equation https://hal.archives-ouvertes.fr/hal-01305360/document.

[5] Cattaneo, C. (1958) Sur une forme d'équation de la chaleur éliminant le paradoxe d'une propagation instantanée, Comptes Rendus de l'Académie des Sciences, **247**, pp. 431433.

[6] Davis, S. F. (1988) Simplified second-order Godunov-type methods. SIAM Journal on Scientific and Statistical Computing, 9(3), 445-473.

[7] Dumbser, M., Peshkov, I., Romenski, E. & Zanotti, O. (2016) High order ADER schemes for a unified first order hyperbolic formulation of continuum mechanics : viscous heat - conducting fluids and elastic solids, J. Comp. Physics, **314**, 824-862.

[8] El, G. A. & Hoefer, M. (2016) Dispersive shock waves and modulation theory, Physica D, **333**, 11-65.

[9] Eringen, A. C. Microcontinuum Field Theories, I: Foundation and Solids, Springer Verlag, 1999.

[10] Favre, H. 1935 Ondes de translation dans les canaux découverts. Dunod (Paris).

[11] Forest, S. (2009) Micromorphic approach for gradient elasticity, viscoplasticity and damage, **135**, 117-131.

[12] Forest, S. (2016) Nonlinear regularisation operators as derived from the micromorphic approach to gradient elasticity, viscoplasticity and domage. Proc. Royal Soc. A **472** : 20150755.

[13] S. Gavrilyuk (1994) Large amplitude oscillations and their "thermodynamics" for continua with "memory", European J. Mechanics, B/Fluids, **13**, N 6, 753-764.

[14] Gavrilyuk, S. L. & Teshukov, V. M. (2001) Generalized vorticity for bubbly liquid and dispersive shallow water equations, Continuum Mechanics and Thermodynamics **13**, 365 - 382.

[15] Gavrilyuk, S. (2011) Multiphase Flow Modeling via Hamilton's principle. In the book : Variational Models and Methods in Solid and Fluid Mechanics, CISM Courses and Lectures, v. 535 (Eds. F. dell'Isola and S. Gavrilyuk), Springer, 2011.

[16] Gavrilyuk, S. L., Liapidevskii, V. Yu. & Chesnokov, A. A. (2016) Spilling breakers in shallow water : applications to Favre waves and to the shoaling and the breaking of the solitary wave (submitted).

[17] Green, A. E., Laws, N. & Naghdi, P. M. (1974) On the theory of water waves. Proc. R. Soc. Lond. A, **338**, 4355.

[18] Green, A. E. & Naghdi, P. M. (1976) A derivation of equations for wave propagation in water of variable depth. J. Fluid. Mechanics, **78**, 237-246.

[19] Hedstrom, G. W. (1979) Nonreflecting Boundary Conditions for Nonlinear Hyperbolic Systems, J. Comp. Physics, **30**, 222-237.

[20] Le Métayer, O., Gavrilyuk, S., & Hank, S. (2010). A numerical scheme for the GreenNaghdi model. Journal of Computational Physics, 229(6), 2034-2045.

[21] Neff, P., Ghiba, I. D., Madeo, A., Placidi, L., and Rosi, G. (2014). A unifying perspective: the relaxed linear micromorphic continuum. Continuum Mechanics and Thermodynamics, 26(5), 639-681.

[22] Lannes, D. & Marche, F. (2015) A new class of fully nonlinear and weakly dispersive Green-Naghdi models for efficient 2D simulations, J. Comp. Physics, **282**, 238 - 268.

[23] Liapidevskii, V. Y., and Gavrilova, K. N. (2008). Dispersion and blockage effects in the flow over a sill. Journal of applied mechanics and technical physics, 49(1), 34-45.

[24] LeVeque, R. J. (2002) Finite volume methods for hyperbolic problems (Vol. 31). Cambridge university press.

[25] Montecinos, G. I., Lopez-Rios, J. C., Lecaros, R., Ortega, J. H. & Toro, E. F. (2016) An ADER-type scheme for a class of equations arising from the water-wave theory, Computers and Fluids **132** 76-93.

[26] Peshkov, I. & Romenski, E. (2016) A hyperbolic model for viscous Newtonian flows. Continuum Mech. Thermodyn. **28**, p. 85-104, DOI 10.1007/s00161-014-0401-6.

[27] Serre, F. (1953) Contribution à l'étude des écoulements permanents et variables dans les canaux. La Houille blanche, **8**, 830872, 1953.

[28] Toro, E. F. (2013) Riemann solvers and numerical methods for fluid dynamics: a practical introduction. Springer Science and Business Media.

[29] Su, C. H. & Gardner, C. S. (1969) Korteweg - de Vries Equation and Generalisations. III. Derivation of the Korteweg - de Vries Equation and Burgers Equation, J. Math. Physics, **10**, 536–539.

[30] Salmon, R. (1998) Lectures on Geophysical Fluid Mechanics, Oxford University Press, 1998.

[31] Treske, A. (1994) Undular bores (favre-waves) in open channels-experimental studies. Journal of Hydraulic Research, 32(3), 355-370.

[32] Whitham, G. B. (1974) Linear and Nonlinear Waves, John Wiley & Sons.